CHEMISTRY OF MATERIALS

Article

pubs.acs.org/cm

High Voltage Mg-Doped $Na_{0.67}Ni_{0.3-x}Mg_xMn_{0.7}O_2$ (x = 0.05, 0.1) Na-Ion Cathodes with Enhanced Stability and Rate Capability

Gurpreet Singh,[†,⊥] Nuria Tapia-Ruiz,[‡,⊥] Juan Miguel Lopez del Amo,[†] Urmimala Maitra,[‡] James W. Somerville,[‡] A. Robert Armstrong,[§] Jaione Martinez de Ilarduya,[†] Teófilo Rojo,*[,†,∥] and Peter G. Bruce*[,‡]

[†]CICenergigune, Parque Tecnológico de Álava, Albert Einstein 48, ED.CIC, 01510 Miñano, Spain

[‡]Department of Materials, University of Oxford, Oxford OX1 3PH, United Kingdom

[§]School of Chemistry, University of St. Andrews, St. Andrews, Fife KY16 9ST, United Kingdom

[∥]Departamento de Química Inorgánica, Universidad del País Vasco UPV/EHU, P.O. Box. 644, 48080 Bilbao, Spain

Supporting Information

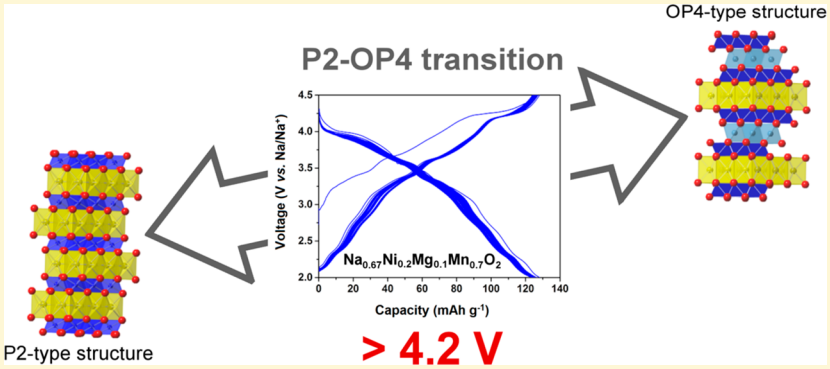

ABSTRACT: Magnesium substituted P2-structure $Na_{0.67}Ni_{0.3}Mn_{0.7}O_2$ materials have been prepared by a facile solid-state method and investigated as cathodes in sodium-ion batteries. The Mg-doped materials described here were characterized by X-ray diffraction (XRD), ^{23}Na solid-state nuclear magnetic resonance (SS-NMR), and scanning electron microscopy (SEM). The electrochemical performance of the samples was tested in half cells vs Na metal at room temperature. The Mg-doped materials operate at a high average voltage of ca. 3.3 V vs Na/Na^+ delivering specific capacities of ~120 mAh g^{-1}, which remain stable up to 50 cycles. Mg doping suppresses the well-known P2−O2 phase transition observed in the undoped composition by stabilizing the reversible OP4 phase during charging (during Na removal). GITT measurements showed that the Na-ion mobility is improved by 2 orders of magnitude with respect to the parent P2−$Na_{0.67}Ni_{0.3}Mn_{0.7}O_2$ material. The fast Na-ion mobility may be the cause of the enhanced rate performance.

INTRODUCTION

Over the last two decades, most of the portable electronic market has been dominated by lithium-ion batteries (LIBs). These batteries are now finding new market opportunities in the electric vehicle industry along with stationary energy storage.[1] Even though the high energy density of lithium-ion batteries makes them attractive for many applications, there is a demand for inexpensive technology for which the sources of the ores are more uniformly distributed across the globe. Sodium-ion batteries (SIBs) are a promising alternative, addressing the aforementioned issues related to the cost and sources. Following their inception in the 1980s these batteries are under reinvestigation as an alternative to LIBs for certain applications.[2−6] Various types of cathode and anode materials have been proposed and studied for SIBs, often mimicking their LIB counterparts. Among cathode materials, layered oxide compounds of the type Na−TM−O_2 (TM = 3d transition metal) have shown promise in terms of energy density and rate capability. The most studied layered compounds can be classified as P2-type and O3-type structures as described by Delmas' notation.[7] P and O refer to the Na coordination, i.e., trigonal prismatic or octahedral, respectively, while the number represents the repeated transition metal oxide stacking within the unit cell (ABBA, ABCABC). Of these two layered structures, P2-type compounds provide great promise as they undergo fewer structural transitions when (de)intercalating Na-ions.[2]

P2−$Na_{2/3}Ni_{1/3}Mn_{2/3}O_2$ was first reported in 2001 by Lu and Dahn.[8,9] This material has a relatively high theoretical capacity (173 mAh g^{-1}), but more importantly, it shows an average

Received: May 13, 2016
Revised: June 27, 2016
Published: June 27, 2016

DOI: 10.1021/acs.chemmater.6b01935
Chem. Mater. 2016, 28, 5087−5094

operating voltage greater than 3.5 V (vs Na/Na^+), attributed to the Ni^{2+}/Ni^{4+} redox couple.[10,11] The main drawback, however, is its poor cycle life, which has been attributed to the detrimental P2−O2 transformation that occurs at high voltages. This transition is caused by gliding of the transition metal layers upon sodium removal.[8,9,12] In order to address the issue of capacity fade, doping of $Na_{0.67}Ni_{0.33}Mn_{0.67}O_2$ with ions such as Zn^{2+} or Ti^{4+} (substituting for Ni and Mn, respectively) has been adopted.[13,14] Doping with these cations increases the amount of sodium left in the structure at the end of charge, alleviating the layer gliding at the expense of capacity. Similarly, Li^+ doping accompanied by an increase in sodium content to 0.85 (i.e., $Na_{0.85}Li_{0.17}Ni_{0.21}Mn_{0.64}O_2$) stabilizes the structure while cycling with reversible capacities of ∼120 mAh g^{-1}.[15] Recent reports in the literature have shown that Mg doping on the transition metal site improved the cycling stability of P2−$Na_{2/3}Mn_{1-x}Mg_xO_2$ ($0 \le x \le 0.2$) while smoothing the charge/discharge voltage profiles.[16] Moreover, further increase in the Mg content led to an abnormally high capacity due to the participation of oxygen anions and/or partial loss of oxygen, although the capacity of the material falls at a faster rate compared with the lightly doped samples.[17] Recent reports, have shown that Mg could also be substituted in the Na−Mn−Ni−O system.[18−20] Even though in these reports the authors have highlighted the suppression of the O2 phase when doping with Mg^{2+}, no identification and characterization of the OP4 phase occurring at high voltages in the Mg-doped materials was made. Here we report a systematic study on effective Mg-doping in the P2−$Na_{0.67}Ni_{0.3}Mn_{0.7}O_2$ system and have shown that in the Mg-doped compounds a reversible P2−OP4 transition occurs at high voltages in contrast to the P2−O2 transition observed in the undoped material. Reducing the Ni content from the typical $Na_{2/3}Ni_{1/3}Mn_{2/3}O_2$ material[8,9] is beneficial from a cost perspective. Increased Mg contents favor Na^+ vacancy disorder upon cycling, which could explain the increased Na-ion mobility observed in these materials.

EXPERIMENTAL SECTION

$Na_{0.67}Ni_{0.3}Mn_{0.7}O_2$ was synthesized as described in ref 12. The Mg-doped samples were synthesized via a solid state synthesis route by mixing the precursors Na_2CO_3 (Sigma-Aldrich, anhydrous ≥99.5%), NiO (Ni 78.5%, Alfa Aesar), Mn_2O_3 (−325 mesh, 99%, Sigma-Aldrich) and MgO (99.99% Alfa Aesar) in appropriate ratios. The powdered mixture was pressed as pellets under a load of 4 tons cm^{-2} before calcining at 900 °C for 12 h in air followed by slow cooling in the furnace. Samples were kept in an Ar filled glovebox maintained at <0.1 ppm of H_2O and O_2.

Powder X-ray diffraction (PXRD) patterns were recorded on a 9 KW Rigaku Smartlab diffractometer using Cu Kα_1 radiation (λ = 1.54051 Å). PXRD data was refined by the Rietveld method using the GSAS software suite with the EXPGUI software interface.[21] A customized airtight sample holder covered with Kapton film was used to avoid severe air/moisture contact during measurement. In situ X-ray diffraction was performed on electrochemical cells equipped with an aluminum-coated beryllium window. The active material (70 wt %) was mixed with carbon black (30 wt %) for 1 h and used in the electrochemical cells for the charge/discharge measurements. X-ray diffraction data were collected using Cu Kα_1 radiation (λ = 1.54051 Å). Each X-ray pattern was collected for 1 h. Metallic sodium was used as counter electrode with 1 M $NaPF_6$ in EC/DEC (1:1 by vol %) as electrolytic solution. The cell was cycled at 5 mA g^{-1} between 2.0 and 4.5 V.

Chemical analyses were performed by inductively coupled plasma (ICP) emission spectroscopy using a PerkinElmer Elan 6100 DRC ICP-MS.

The sample morphology was determined using scanning electron microscopy (SEM, Zeiss Merlin Analytical) at 1 kV and 84 μA.

Ni and Mn K-edge X-ray absorption spectra (XAS) were collected in transmission mode at the B18 Core EXAFS beamline at Diamond Light Source. Reference spectra were simultaneously collected for each measurement using Ni and Mn metal foil. Three scans were collected for each sample and the data were averaged. The Ifeffit software analysis suite was used for the background corrections and normalisation (Athena).[22]

^{23}Na magic angle spinning nuclear magnetic resonance (MAS NMR) experiments were performed at 52.9 MHz, on a Bruker-300 spectrometer charged to a field of 4.7 T. A 1.3 mm standard probe head was used, and the rotor MAS spinning speed used was 50 kHz in all cases. A rotor synchronized spin−echo pulse sequence (90°−τ−180°−τ1−acquisition) was used with typical 90° and 180° pulses of 1.2 and 2.4 μs, respectively, and the recycle delay was set to 0.8 s. The spectra were referenced to a 0.1 M solution of $^{23}NaCl$. The fitting of the ^{23}Na NMR signals were performed using the Dmfit software.[23]

Electrode preparation involved mixing the active material with conductive carbon black and PVDF (polyvinylidene fluoride) as binder in the ratio of 75:15:10, respectively. Slurries were prepared by adding a few drops of NMP (*n*-methyl-2-pyrrolidone) to the mixture under constant stirring for 30 min. The slurry was cast onto Al foil that acts as current collector. Loading of active material for the galvanostatic cycling is 5.81 mg cm^{-2} and for GITT measurements is 2 mg cm^{-2}. The coated foil was dried under vacuum at 120 °C for 2 h and electrodes of desired diameter were punched out and pressed under a load of 4 tons cm^{-2}. Galvanostatic cycling was performed in CR2032 coin cells, where metallic sodium was used as counter electrode with glass fiber filter paper (Whatman) as separator and 1 M $NaPF_6$ (99.99% Sigma-Aldrich) in EC/DEC (1:1 by vol%) as the electrolyte. Electrochemical cells were charged/discharged at different current rates between 2 and 4.5 V. AC impedance spectroscopy was carried out in a VMP3 (Bio Logic) in the frequency range 200 kHz to 5 mHz. Measurements were conducted in a 2-electrode cell (coin-cell type) with an AC signal amplitude of 10 mV.

RESULTS AND DISCUSSION

Figure 1 shows the refined powder X-ray diffraction (PXRD) plots of $Na_{0.67}Ni_{0.3-x}Mg_xMn_{0.7}O_2$, where x = 0.05 (a) and x = 0.1 (b). Table 1 shows the relevant crystallographic data obtained from the Rietveld refinements. For comparison, refinement data on the undoped material are also shown in the SI. Detailed inspection of PXRD data showed extra reflections at 20° 2θ (not shown here) from the honeycomb $\sqrt{3}a \times \sqrt{3}a$ in-plane ordering typically seen in Mg^{2+}/Mn^{4+} systems.[15] By contrast, the observation of Ni^{2+}/Mn^{4+} ordering is difficult by PXRD as the X-ray scattering factors of Ni and Mn are very similar. The similar refined lattice parameters observed in these samples suggest that the long-range structure remains unaltered when increasing from x = 0.05 to 0.1 (Table 1). Transition metal occupancy factors were fixed using the nominal stoichiometry, which matched, in turn, the values obtained from ICP (Table 2). Slightly larger SOF were observed for Na_e sites (edge-shared) since these are energetically more favorable from the electrostatic point of view than the Na_f site (face-shared).

The morphological features and particle size of the pristine materials were determined by scanning electron microscopy (SEM). SEM micrographs showed irregular particles with hexagonal platelet shapes and sizes ranging between 1 and 5 μm (Figure 2). The ^{23}Na solid state NMR spectra of $Na_{0.67}Ni_{0.3-x}Mg_xMn_{0.7}O_2$ (x = 0, 0.05, and 0.1) are shown in Figure 3. The spectra are characterized by a main signal centered at around 1420 ppm corresponding to the central transition of one or more ^{23}Na NMR signals broadened by

DOI: 10.1021/acs.chemmater.6b01935
Chem. Mater. 2016, 28, 5087−5094

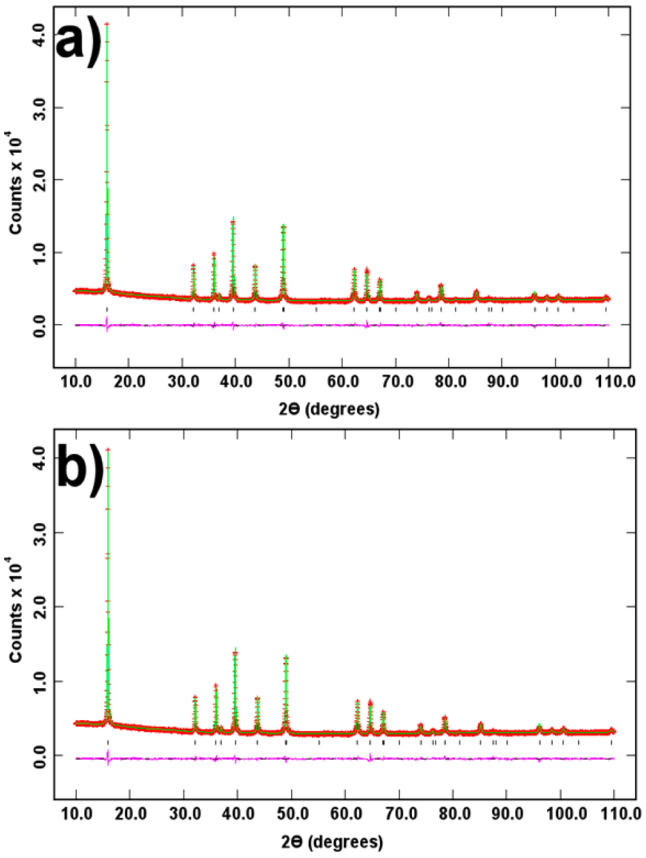

Figure 1. Fitted powder X-ray diffractograms at room temperature for $Na_{0.67}Ni_{0.3-x}Mg_xMn_{0.7}O_2$ where x = 0.05 (a); and x = 0.1 (b). Observed data are shown in red, calculated data are shown in green, and the difference between the two profiles is shown in pink. Black tick marks indicate Bragg reflections from the calculated data.

second order quadrupolar interactions. The two minor symmetric signals marked by asterisks in the spectra are rotational side bands, and the signal at around 0 ppm corresponds to a minor diamagnetic Na_2CO_3 impurity of the sample.[24−26] The quadrupolar features observed in the ^{23}Na NMR spectrum of P2−$Na_{0.67}Ni_{0.3}Mn_{0.7}O_2$ (black) are indicative of a high degree of structural ordering in the material. As previously discussed by Cabana and co-workers,[24] the ^{23}Na NMR spectrum of this compound cannot be satisfactorily fitted considering a single line, consistent with

Table 2. Nominal Compositions for $Na_{0.67}Ni_{0.3-x}Mg_xMn_{0.7}O_2$ (x = 0.05 and 0.1) Obtained from ICP Measurements

	molar fraction[a]	
	x = 0.05	x = 0.1
M	$Na_{0.66}Ni_{0.26}Mg_{0.04}Mn_{0.7}O_2$	$Na_{0.67}Ni_{0.20}Mg_{0.09}Mn_{0.71}O_2$
Na	0.66	0.67
Ni	0.26	0.20
Mn	0.70	0.71
Mg	0.04	0.09

[a]Errors are within 5% of the values given.

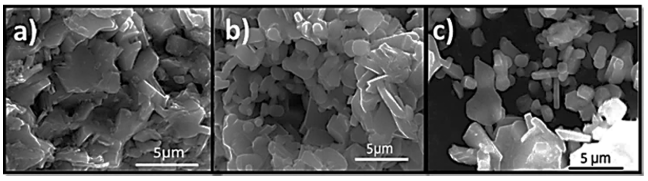

Figure 2. SEM images of (a) $Na_{0.67}Ni_{0.3}Mn_{0.7}O_2$, (b) $Na_{0.67}Ni_{0.25}Mg_{0.05}Mn_{0.7}O_2$, and (c) $Na_{0.67}Ni_{0.2}Mg_{0.1}Mn_{0.7}O_2$, showing a platelet-like morphology with average particle size in the 1−5 μm.

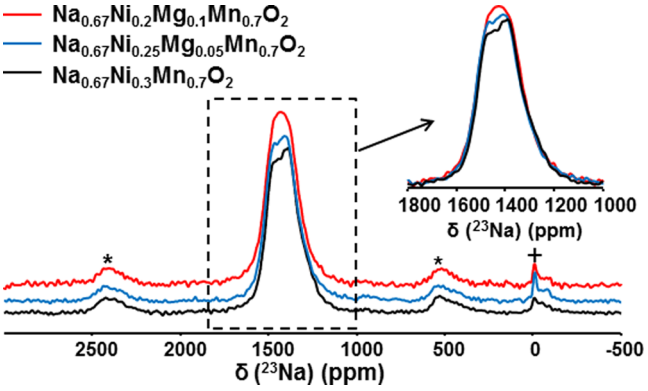

Figure 3. ^{23}Na NMR spectra of $Na_{0.67}Ni_{0.3-x}Mg_xMn_{0.7}O_2$ (x = 0, 0.05, and 0.1). The second order quadrupolar features observed in the spectrum of $Na_{0.67}Ni_{0.3}Mn_{0.7}O_2$ disappear gradually as the level of Mg is increased, in agreement with a reduction of the structural ordering of the Na^+ ions in the structure.

the presence of more than one Na^+ site in the alkali layers of the structure. Although an unambiguous fitting of the spectrum would require the measurement of the NMR signal at different

Table 1. Selected Rietveld Refinement Data from X-Ray Data at Room Temperature for $Na_{0.67}Ni_{0.3-x}Mg_xMn_{0.7}O_2$ (x = 0.05 and 0.1)

sample	atom	Wyckoff position	X	Y	Z	SOF	B_{iso} (Å^2)
x = 0.05	Na(e)	2d	2/3	1/3	0.25	0.374(1)	2.8 (1)
a = 2.88482(2) Å	Na(f)	2b	0	0	0.25	0.296(1)	1.2 (1)
c = 11.1583(2) Å	Ni/Mn/Mg	2a	0	0	0	0.25/0.7/0.05	2.51(4)
χ^2 = 1.806							
R_p = 1.70%	O	4f	2/3	1/3	0.0898(1)	1	2.82(1)
R_{pw} = 2.29%							
x = 0.1	Na(e)	2d	2/3	1/3	0.25	0.403(2)	3.8(1)
a = 2.88482(3) Å	Na(f)	2b	0	0	0.25	0.267(2)	1.0(1)
c = 11.1587(2) Å	Ni/Mn/Mg	2a	0	0	0	0.2/0.7/0.1	2.94(2)
χ^2 = 2.301							
R_p = 1.78%	O	4f	2/3	1/3	0.0912(1)	1	3.34(6)
R_{pw} = 2.55%							

DOI: 10.1021/acs.chemmater.6b01935
Chem. Mater. 2016, 28, 5087−5094

fields, an accurate fit is possible considering two ^{23}Na populations with the relative intensities obtained from the Rietveld refinement on the PXRD data (Table 1). The result of this fitting is shown in Figure S2.

It is clear from the inspection of the inset of Figure 3 that the quadrupolar features observed in the spectrum of P2−$Na_{0.67}Ni_{0.3}Mn_{0.7}O_2$ vanish gradually when the level of Mg^{2+} doping is increased progressively to 0.05 and 0.1. Mg^{2+} ions favor the presence of new Na^+ environments, which result in broadening of the ^{23}Na NMR signals observed in Figure 3, and the subsequent disappearance of the quadrupolar features. The ^{23}Na NMR broadening can be additionally induced by the increased Na^+ mobility in the Mg doped phases (as will be described below).

The ^{23}Na NMR shifts observed for the central transition in Figure 3 are very large, as expected by the presence of Na−O−M (M = Ni, Mn) hyperfine interactions with paramagnetic centers, in agreement with the spectra previously recorded by Cabana et al. for the $Na_xNi_{x/2}Mn_{1-x/2}O_2$ family.[24] The hyperfine interactions generating such large shifts are very sensitive to variations in Na−O−M distances and angles, and the signs of the interactions can be positive or negative with variable magnitudes depending on the local geometries of the orbitals and the number of unpaired electrons involved in the interaction. Although the replacement of a paramagnetic Ni^{2+} ion in the structure by an Mg^{2+} cation with no unpaired electron density should, in principle, give rise to a signal with a different shift in the NMR spectrum, no significant changes in the ^{23}Na NMR shifts are observed for the different spectra of Figure 3. Similar observations were made for the ^{23}Na NMR shifts of the $Na_xNi_{x/2}Mn_{1-x/2}O_2$ polytype and for the ^{6}Li NMR signals in $Li_xNi_{x/2}Mn_{1-x/2}O_2$. Very subtle variations of shifts were observed in both cases despite the different Mn^{4+}/Ni^{2+} ratios.[24] These results were explained by the small variations of interlayer spacing in these compounds that result in different strengths of the Fermi contact interaction that compensate the different paramagnetism in Mn^{4+}/Ni^{2+}.

The electrochemical performance of the various samples has been evaluated in the voltage range of 2.0−4.5 V. Three plateaus at ∼3.3, ∼3.7, and ∼4.2 V were observed during the first charge cycle of the undoped sample, which are in agreement with those reported in the literature on $Na_{2/3}Ni_{1/3}Mn_{2/3}O_2$.[12] Charge/discharge curves of the pristine material are shown in Figure 4a. An initial charge capacity of ∼150 mAh g^{-1} (removal of 0.59 Na^+) was observed at 12 mA g^{-1} corresponding to the oxidation of Ni^{2+}. It can be observed from the figure that the plateau at ∼4.2 V, which corresponds to the evolution of the O2 phase (0.31 Na^+ removed),[9] diminished over 50 cycles. The discharge capacity drops from 120 to 56 mAh g^{-1} over the course of 50 cycles. The drop in the capacity is mainly attributed to the disappearance of the highest voltage process. This is in agreement with earlier studies on $Na_{2/3}Ni_{1/3}Mn_{2/3}O_2$.[12] Galvanostatic charge/discharge profiles of $Na_{0.67}Ni_{0.25}Mg_{0.05}Mn_{0.7}O_2$ and $Na_{0.67}Ni_{0.2}Mg_{0.1}Mn_{0.7}O_2$ compositions are shown in Figure 4b,c, respectively. Table 3 summarizes the electrochemical data obtained from the doped samples. Even though the voltage steps that were observed in the pristine samples at ∼3.3, ∼3.7, and ∼4.2 V are visible, in the Mg^{2+} doped compositions they are suppressed to a larger extent with Mg content. With the doping of Mg^{2+} ions in the structure, the initial charge capacity falls from 150 mAh g^{-1} for the undoped sample to 136 mAh g^{-1} for x = 0.05 (0.52 Na^+ removed). This may be attributed to the replacement of the electrochemically active Ni^{2+} ions with electrochemically inactive Mg^{2+} ions. X-ray absorption was used to probe the changes in oxidation state of Ni and Mn upon cycling. From

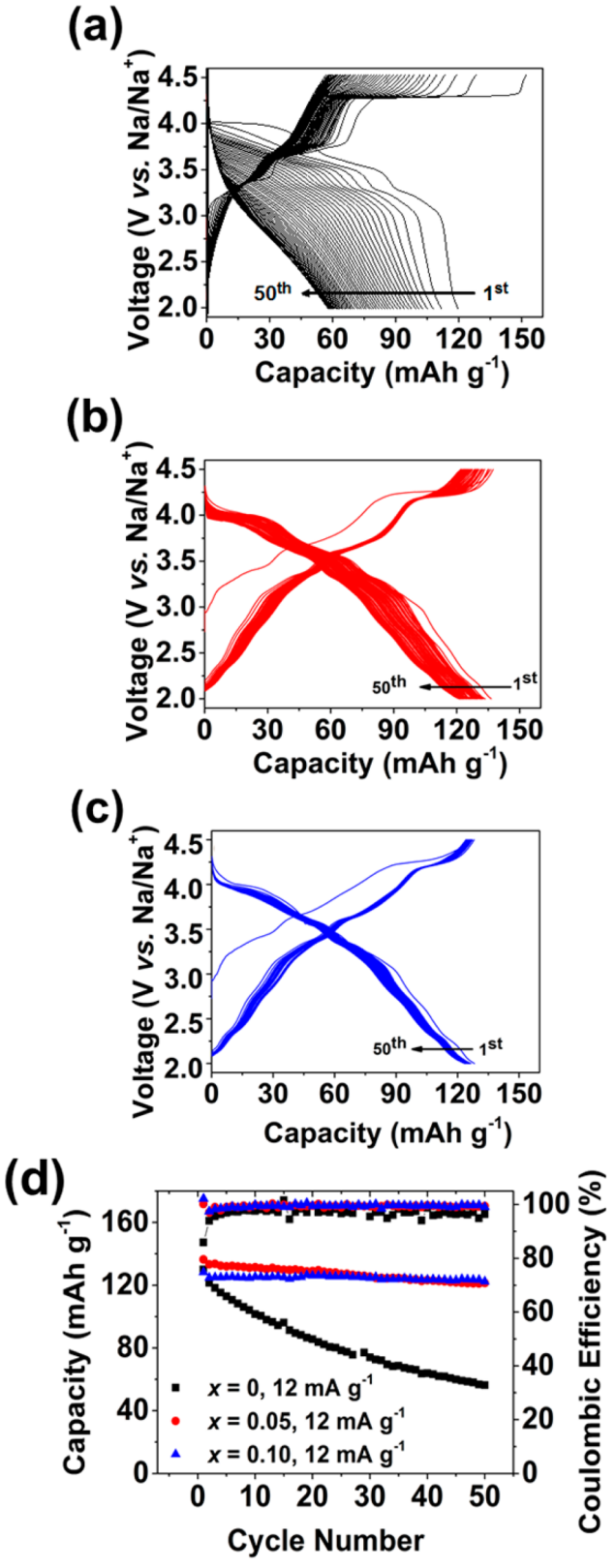

Figure 4. Galvanostatic charge/discharge curves in the 2−4.5 V range at 12 mA g^{-1} showing 50 cycles for (a) $Na_{0.67}Ni_{0.3}Mn_{0.7}O_2$, (b) $Na_{0.67}Mg_{0.05}Ni_{0.25}Mn_{0.7}O_2$, and (c) $Na_{0.67}Mg_{0.1}Ni_{0.2}Mn_{0.7}O_2$. (d) Capacities and Coulombic efficiency of the samples vs cycle number.

DOI: 10.1021/acs.chemmater.6b01935
Chem. Mater. 2016, 28, 5087−5094

Table 3. Summary of Electrochemical Data for $Na_{0.67}Ni_{0.3-x}Mg_xMn_{0.7}O_2$ (x = 0.05 and 0.1) Samples at Different Current Rates

current (mA g^{-1})		x = 0.05	x = 0.1
12	initial discharge capacity (mAh g^{-1})	136.4	128.2
	discharge capacity after 50 cycles (mAh g^{-1})	121.4	122.4
	capacity retention (%)	89.0	95.4
200	initial discharge capacity (mAh g^{-1})	124.5	128.6
	discharge capacity after 50 cycles (mAh g^{-1})	113.9	123.7
	capacity retention (%)	91.5	96.2
400	initial discharge capacity (mAh g^{-1})	110.6	118.1
	discharge capacity after 50 cycles (mAh g^{-1})	95.0	111.7
	capacity retention (%)	85.9	94.6

the results we can establish that the capacity mainly originates from the redox active Ni^{2+}/Ni^{4+} couple. Small changes in the manganese K edge associated with the Mn^{3+}/Mn^{4+} redox couple were observed (Figures S3 and S4). A further drop in the initial charge capacity to ~128 mAh g^{-1} (0.48 Na^+ removed) is observed when x = 0.1. For x = 0.05, the discharge capacity drops from 136 to 121 mAh g^{-1} after 50 cycles at a rate of 12 mA g^{-1}, which corresponds to ~90% of capacity retention. For x = 0.1, the discharge capacity falls from 128 to 122 mAh g^{-1} after 50 cycles, which corresponds to 95% of the initial capacity. For all compositions an average operating voltage of ~3.3 V was observed. Evolution of the capacity with the cycle life is shown in Figure 4d. Ex situ X-ray diffraction was carried out after 50 charge/discharge cycles. Cells were opened after discharging the samples to 2.0 V. X-ray diffraction patterns of the Mg-doped samples after 50 cycles are shown in Figure S5. Lattice parameters of the $Na_{0.67}Ni_{0.2}Mg_{0.1}Mn_{0.7}O_2$ material (Table S3) remained almost identical after 50 cycles, whereas for the undoped sample a large increase in the c parameter was observed due to sodium loss upon cycling.

In situ X-ray diffraction of P2−$Na_{0.67}Ni_{0.33}Mn_{0.67}O_2$ has been reported in previous studies showing the structural evolution as Na ions are removed and reinserted in the material.[9] The structure changes from P2 to O2 as the cell voltage reaches ~4.25 V, as shown by the evolution of the characteristic (002) peak present Figure 4. Galvanostatic charge/discharge curves in the 2−4.5 V near $2\theta \approx 20°$. An identical phase transition has been observed in the undoped $Na_{0.67}Ni_{0.3}Mn_{0.7}O_2$ material studied here (Figure S6). In order to study the effects of Mg on the structure upon cycling, we have performed in situ PXRD measurements on the x = 0.1 doped sample (i.e., $Na_{0.67}Ni_{0.2}Mg_{0.1}Mn_{0.7}O_2$, Figure 5). Changes in the a and c lattice parameters upon cycling are shown in Figure S7 and Table S2. No characteristic peak corresponding to the O2 phase is observed in the high voltage region (4.2−4.5 V). However, evolution of a clear broad peak as a shoulder on the highest intensity peak corresponding to the P2 phase is observed at ca. 0.35 Na content. This broad peak is characteristic of the OP4 phase, which has been described previously as an intergrowth structure between the P2- and O2-type structures.[16] From these results we believe that the suppression of the P2−O2 phase transition in the Mg-doped sample is responsible for the excellent cycling performance. In fact, several authors have related the P2−OP4 transition to enhanced electrochemical performance.[16,27]

To further analyze the galvanostatic charge/discharge curves we have calculated the derivative of the capacity with respect to voltage. The differential capacity plots are shown in Figure S8. Peaks corresponding to different voltage plateaus in the galvanostatic charge/discharge curves were observed in the

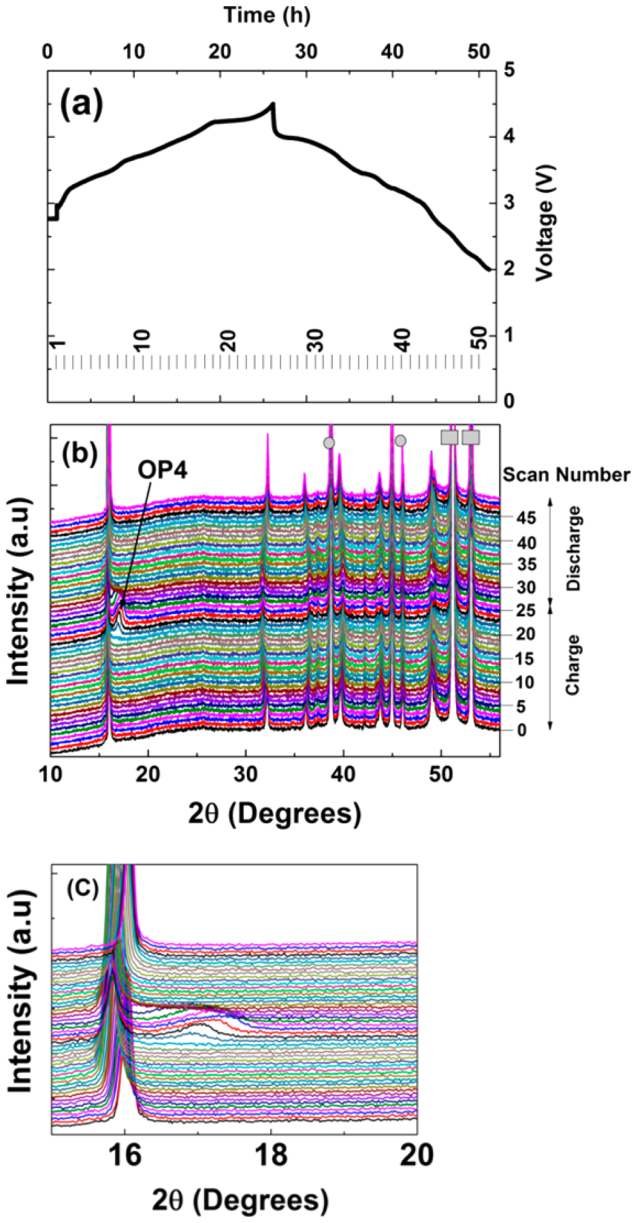

Figure 5. (a) Galvanostatic charge/discharge curves (1st cycle) and (b) in situ powder X-ray diffraction of $Na_{0.67}Ni_{0.2}Mg_{0.1}Mn_{0.7}O_2$ showing the reversible evolution of P2−OP4 phase transition at the end of the charge and beginning of the discharge. (c) Zoomed region showing (002) reflection and OP4 phase. In (b) ■ shows the peaks corresponding to the Be window used and ● corresponds to the presence of the Al current collector. Each X-ray diffraction pattern was collected for 1 h.

DOI: 10.1021/acs.chemmater.6b01935
Chem. Mater. 2016, 28, 5087−5094

differential capacity plots. The oxidation peak at ~4.25 V is attributed to the P2−O2 phase transition in the pristine sample (Figure S8a). The reduction peak corresponding to the O2−P2 phase transition appears at ~4.0 V. This peak disappears and shifts to lower potential with cycling, showing damage to the crystal structure caused by this phase transition. By contrast, in the doped samples, from the second cycle onward, no significant change in the peak position or intensity is observed. This could be due to the suppression of the P2−O2 phase transition by Mg doping and consequent formation of the more reversible OP4 phase at high voltages (Figure S8b,c).

This demonstrates the significant stabilizing effect of the Mg^{2+} ions in the structure. The differential capacity plots of the doped samples show additional peaks at low voltages, which are attributed to Mn^{3+}/Mn^{4+} redox processes. The theoretical capacity based on Ni^{2+}/Ni^{4+} is slightly lower than the experimentally observed capacity, which is further evidence of the activation of the Mn^{3+}/Mn^{4+} redox couple in these materials.

The rate capability of the materials is shown in Figure 6, where it is apparent that the Mg doping increases the rate

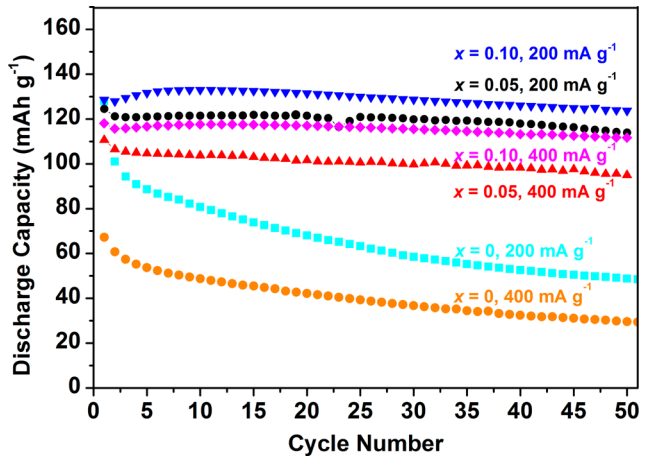

Figure 6. Cycling data of $Na_{0.67}Ni_{0.3-x}Mg_xMn_{0.7}O_2$ (x = 0, 0.05, and 0.1) over 50 cycles. Samples were discharged at 200 and 400 mA g^{-1} and slowly charged at 10 mA g^{-1}.

performance and capacity retention if compared to the undoped material. For x = 0.1, the initial discharge capacity decreases from 128 to 118 mAh g^{-1} (92% retention) when the rate is increased 2-fold from 200 to 400 mA g^{-1}. Additional electrochemical data is shown in Table 3. Ex situ XRD data $Na_{0.67}Ni_{0.3-x}Mg_xMn_{0.7}O_2$ (x = 0.05 and 0.1) after 50 cycles (charged at 10 mA g^{-1} and discharged at 200 and 400 mA g^{-1}) are shown in Figures S9 and S10. XRD patterns of both samples could be indexed to the pristine materials described above, showing the robustness of these structures upon cycling. The broadening observed in the peaks was attributed to large concentration gradients across the particles caused by the high stress produced in the materials when cycling at fast rates (Table S4).

The enhanced rate capability of the Mg-doped compounds described here was further investigated using galvanostatic intermittent titration methods (GITT). GITT measurements were also conducted on as-synthesized P2−$Na_{0.67}Ni_{0.3}Mn_{0.7}O_2$ for further comparison (Figures S11−S13). For GITT measurements a pulse of 1.7 μA was applied for 1 h followed by a relaxation time of 2 h. Figure 7 shows the variation of the

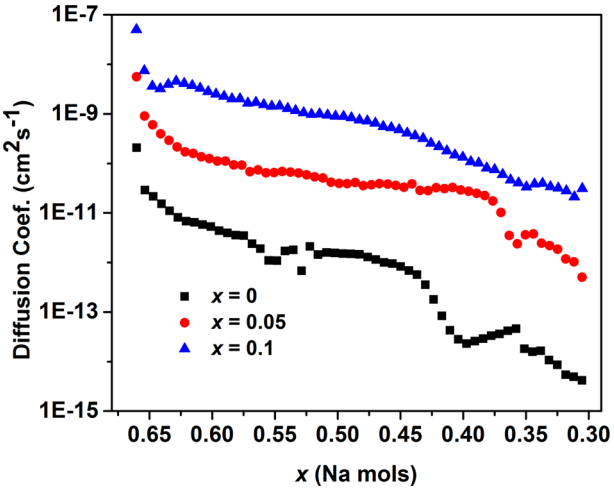

Figure 7. Na diffusion coefficients (D_{Na}^+) calculated from GITT measurements in P2−$Na_{0.67}Ni_{0.3}Mn_{0.7}O_2$ (black), $Na_{0.67}Ni_{0.25}Mg_{0.05}Mn_{0.7}O_2$ (red), and $Na_{0.67}Ni_{0.2}Mg_{0.1}Mn_{0.7}O_2$ (blue) as a function of the Na concentration remaining in the structure.

Na diffusion coefficient (D_{Na}^+) in the studied samples determined from the GITT profiles. The D_{Na}^+ is calculated using equation S(i) (see SI). Na-ion mobility in $Na_{0.67}Ni_{0.2}Mg_{0.1}Mn_{0.7}O_2$ is the highest of all the materials described here, with diffusion coefficients ranging from 10^{-7} to 10^{-10} cm^2 s^{-1} in the Na range $0.67 \geq x \geq 0.33$. Comparable sodium diffusion coefficients were obtained by AC impedance in order to validate these results (Figure S14). Li et al. have also observed improved high-rate performance in the Mg- and Ni-doped $Na_{0.67}MnO_2$ with formula $Na_{0.67}Ni_{0.1}Mg_{0.1}Mn_{0.8}O_2$ and explained this with the expansion of the interplanar spacing of the sodium layer caused by shortening of the TM−O bond lengths and the shrinkage of the TMO_6 octahedra.[19] These observations may be caused by the greater Na disorder caused by the increased Mg content in the transition metal layers. P2−$Na_{0.67}Ni_{0.25}Mg_{0.05}Mn_{0.7}O_2$ showed diffusion coefficients of 10^{-8} to 10^{-10} cm^2 s^{-1} within the same range of sodium contents. These values are higher than those reported by Mendiboure et al. in P2−$Na_{0.70}MnO_2$ and P2−$Na_{0.7}CoO_2$ of 1.7×10^{-14} and 5×10^{-12} cm^2 s^{-1}, respectively.[28] Interestingly, no jumps in the Na diffusion coefficient values, attributed to sodium ordering in the undoped compound,[29] were observed for x = 0.05 and x = 0.1. Hence the results are in agreement with the smoothing of the load curves observed in these materials. The abrupt decrease in Na-ion mobility in the doped samples at high potentials (low Na^+ contents ~0.35) could be explained by the formation of the OP4 structure caused by gliding of the transition metal layers leading to octahedral Na^+ vacancies.

CONCLUSIONS

Magnesium doping in P2−$Na_{0.67}Ni_{0.3}Mn_{0.7}O_2$ enhances the cyclability and rate performance of the material in the 2−4.5 V range. Doping the structure with Mg^{2+} led to the formation of the OP4 phase at high voltages, and the P2−OP4 phase transition is observed to be highly reversible as reflected by the X-ray diffraction data. The sodium-ion mobility is observed to improve with Mg doping. Na-ion mobility in $Na_{0.67}Ni_{0.2}Mg_{0.1}Mn_{0.7}O_2$ is the highest of all the materials discussed in this study, with diffusion coefficients as high as 10^{-7} cm^2 s^{-1}. Excellent capacity retention (~95% of initial (128 mAh g^{-1})) over 50 cycles with an average operating voltage

DOI: 10.1021/acs.chemmater.6b01935
Chem. Mater. 2016, 28, 5087−5094

~3.3 V vs Na/Na^+ makes $Na_{0.67}Ni_{0.2}Mg_{0.1}Mn_{0.7}O_2$ very interesting as a potential candidate for the sodium ion batteries.

■ ASSOCIATED CONTENT

Supporting Information

The Supporting Information is available free of charge on the ACS Publications website at DOI: 10.1021/acs.chemmater.6b01935.

Rietveld plot; ^{23}Na NMR data; X-ray absorption spectra; ex situ PXRD patterns; in situ X-ray data; variation of lattice parameters; differential capacity plots; ex situ PXRD data; GITT profiles; impedance spectrum; selected Rietveld refinement data; refined lattice parameters and fraction of OP4 phase; calculated fwhm (PDF)

■ AUTHOR INFORMATION

Corresponding Authors

*E-mail: peter.bruce@materials.ox.ac.uk.
*E-mail: trojo@cicenergigune.com.

Author Contributions

⊥G.S. and N.T.R. contributed equally to this work. The manuscript was written by G.S. and N.T.R. through contributions of all authors. The project was supervised by G.S., N.T.R., and P.G.B.

Notes

The authors declare no competing financial interest.
Research data has been deposited in ORA-data at DOI: 10.5287/bodleian:aZjEYwA0b.

■ ACKNOWLEDGMENTS

At CIC Energigune this work was financially supported by LINABATT project from Ministerio de Economía Competitividad (ENE2013-44330-R). P.G.B. (University of Oxford) is indebted to the Engineering and Physical Sciences Research Council, including the SUPERGEN program, for financial support.

■ REFERENCES

(1) Larcher, D.; Tarascon, J. M. Towards greener and more sustainable batteries for electrical energy storage. *Nat. Chem.* **2015**, *1*, 19−29.

(2) Palomares, V.; Serras, P.; Villaluenga, I.; Hueso, K. B.; Carretero-González, J.; Rojo, T. Na-ion batteries, recent advances and present challenges to become low cost energy storage systems. *Energy Environ. Sci.* **2012**, *5*, 5884−5901.

(3) Kundu, D.; Talaie, E.; Duffort, V.; Nazar, L. F. The emerging chemistry of sodium ion batteries for electrochemical energy storage. *Angew. Chem., Int. Ed.* **2015**, *54*, 2−20.

(4) Ellis, B. L.; Nazar, L. F. Sodium and sodium-ion energy storage batteries. *Curr. Opin. Solid State Mater. Sci.* **2012**, *16*, 168−177.

(5) Kim, S.-W; Seo, D.-H.; Ma, X.; Ceder, G.; Kang, K. Electrode materials for rechargeable sodium-ion batteries: potential alternatives to current lithium-ion batteries. *Adv. Energy Mater.* **2012**, *2*, 710−721.

(6) Palomares, V.; Casas-Cabanas, M.; Castillo-Martínez, E.; Han, M. H.; Rojo, T. Update on Na-based battery materials. A growing research path. *Energy Environ. Sci.* **2013**, *6*, 2312−2337.

(7) Delmas, C.; Fouassier, C.; Hagenmuller, P. Structural classification and properties of the layered oxides. *Physica B+C* **1980**, *99*, 81−85.

(8) Lu, Z.; Dahn, J. R. Can all the lithium be removed from T2-$Li_{2/3}[Ni_{1/3}Mn_{2/3}]O_2$? *J. Electrochem. Soc.* **2001**, *148*, A710−A715.

(9) Lu, Z.; Dahn, J. R. In-situ X-ray diffraction study of P2-$Na_{2/3}[Ni_{1/3}Mn_{2/3}]O_2$. *J. Electrochem. Soc.* **2001**, *148*, A1225−A1229.

(10) Talaie, E.; Duffort, V.; Smith, H. L.; Fultz, B.; Nazar, L. F. Structure of the high-voltage phase of layered P2-$Na_{2/3-z}[Mn_{1/2}Fe_{1/2}]O_2$ and the positive effect of Ni substitution on its stability. *Energy Environ. Sci.* **2015**, *8*, 2512.

(11) Hasa, I.; Buchholz, D.; Passerini, S.; Hassoun, J. A comparative study of layered transition metal oxide cathodes for application in sodium-ion battery. *ACS Appl. Mater. Interfaces* **2015**, *7*, 5206−5212.

(12) Lee, D. H.; Xu, J.; Meng, Y. S. An advanced cathode for Na-ion batteries with high rate and excellent structural stability. *Phys. Chem. Chem. Phys.* **2013**, *15*, 3304−3312.

(13) Yoshida, H.; Yabuuchi, N.; Kubota, K.; Ikeuchi, I.; Garsuch, A.; Schulz-Dobrickb, M.; Komaba, S. P2-type $Na_{2/3}Ni_{1/3}Mn_{2/3-x}Ti_xO_2$ as a new positive electrode for higher nergy Na-ion batteries. *Chem. Commun.* **2014**, *50*, 3677−3680.

(14) Wu, X.; Guo, J.; Wang, D.; Zhong, G.; McDonald, M. J.; Yang, Y. P2-type $Na_{0.66}Ni_{0.33-x}Zn_xMn_{0.67}O_2$ as new high-voltage cathode materials for sodium-ion batteries. *J. Power Sources* **2015**, *281*, 18−26.

(15) Kim, D.; Kang, S.-H.; Slater, M.; Rood, S.; Vaughey, J. T.; Karan, N.; Balasubramanian, M.; Johnson, C. S. Enabling sodium batteries using lithium-substituted sodium layered transition metal oxide cathodes. *Adv. Energy Mater.* **2011**, *1*, 333−336.

(16) Billaud, J.; Singh, G.; Armstrong, A. R.; Gonzalo, E.; Roddatis, V.; Armand, M.; Rojo, T.; Bruce, P. G. $Na_{0.67}Mn_{1-x}Mg_xO_2$ ($0 \le x \le 0.2$): a high capacity cathode for sodium-ion batteries. *Energy Environ. Sci.* **2014**, *7*, 1387−1391.

(17) Yabuuchi, N.; Hara, R.; Kubota, K.; Paulsen, J.; Kumakura, S.; Komaba, S. New electrode material for rechargeable sodium batteries: P2-type $Na_{2/3}[Mg_{0.28}Mn_{0.72}]O_2$ with anomalously high reversible capacity. *J. Mater. Chem. A* **2014**, *2*, 16851−16855.

(18) (a) Zhao, W.; Kirie, H.; Tanaka, A.; Unnoa, M.; Yamamoto, S.; Noguchi, H. Synthesis of metal ion substituted P2-$Na_{2/3}Ni_{1/3}Mn_{2/3}O_2$ cathode material with enhanced performance for Na ion batteries. *Mater. Lett.* **2014**, *135*, 131−134. (b) Hemalatha, K.; Jayakumar, M.; Bera, P.; Prakash, A. S. Improved electrochemical performance of $Na_{0.67}MnO_2$ through Ni and Mg substitution. *J. Mater. Chem. A* **2015**, *3*, 20908−20912. (c) Ikeuchi, I.; Kubota, K.; Yabuuchi, N.; Komaba, S. Impacts of Mg and Al substitution on $Na_{2/3}Ni_{1/3}Mn_{2/3}O_2$ as positive electrode materials for Na-ion batteries. Abstract MA2014−04 235, IMLB 2014.

(19) Li, Z.-Y.; Gao, R.; Zhang, J.; Zhang, X.; Hu, Z.; Liu, X. New insights into designing high-rate performance cathode materials for sodium ion batteries by enlarging the slab-spacing of the Na-ion diffusion layer. *J. Mater. Chem. A* **2016**, *4*, 3453−3461.

(20) Wang, P.-F.; You, Y.; Yin, Y.-X.; Wang, Y.-S.; Wan, L.-J.; Gu, Li.; Guo, Y.-G. Suppressing the P2-O2 phase transtion of Na0.67Mn0.67-Ni0.33O2 by Magnesium Substitution for Improved Sodium-ion Batteries. *Angew. Chem., Int. Ed.* **2016**, *55*, 7445 in press..

(21) (a) Larson, A. C.; Von Dreele, R. B. General Structural Analysis System (GSAS). *Los Alamos National Laboratory Report LAUR* **1994**, 86−748. (b) Toby, B. H. EXPGUI, a graphical user interface for GSAS. *J. Appl. Crystallogr.* **2001**, *34*, 210−213.

(22) Ravel, B.; Newville, M. Athena, Artemis, Hephaestus: data analysis for X-ray absorption spectroscopy using IFEFFIT. *J. Synchrotron Radiat.* **2005**, *12*, 537−541.

(23) Massiot, D.; Fayon, F.; Capron, M.; King, I.; Le Calvé, S.; Alonso, B.; Durand, J. O.; Bujoli, B.; Gan, Z.; Hoatson, G. Modelling one and two-dimensional solid-state NMR spectra. *Magn. Reson. Chem.* **2002**, *40*, 70−76.

(24) Cabana, J.; Chernova, N. A.; Xiao, J.; Roppolo, M.; Aldi, K. A.; Whittingham, M. S.; Grey, C. P. Study of the transition metal ordering in layered $Na(x)Ni(x/2)Mn(1-x/2)O_2$ ($2/3 \le x \le 1$) and consequences in Na/Li exchange. *Inorg. Chem.* **2013**, *52*, 8540−8550.

(25) Singh, G.; Lopez del Amo, J. M.; Galceran, M.; Perez Villar, S.; Rojo, T. Structural evolution during sodium deintercalation/intercalation in $Na_{2/3}[Fe_{1/2}Mn_{1/2}]O_2$. *J. Mater. Chem. A* **2015**, *3*, 6954−6961.

(26) Gonzalo, E.; Han, M. H.; Lopez del Amo, J. M.; Acebedo, B.; Casas-Cabanas, M.; Rojo, T. Synthesis and characterization of pure P2-

DOI: 10.1021/acs.chemmater.6b01935
Chem. Mater. 2016, 28, 5087−5094

and O3- $Na_{2/3}Fe_{2/3}Mn_{1/3}O_2$ as cathode materials for Na ion batteries. *J. Mater. Chem. A* **2014**, *2*, 18523−18530.
(27) Yabuuchi, N.; Kajiyama, M.; Iwatate, J.; Nishikawa, H.; Hitomi, S.; Okuyama, R.; Usui, R.; Yamada, Y.; Komaba, S. P2-type $Na_x[Fe_{1/2}Mn_{1/2}]O_2$ made from earth-abundant elements for rechargeable Na batteries. *Nat. Mater.* **2012**, *11*, 512−517.
(28) Mendiboure, A.; Delmas, C.; Hagenmuller, P. Electrochemical intercalation and deintercalation of Na_xMnO_2. *J. Solid State Chem.* **1985**, *57*, 323−331.
(29) Shu, G. J.; Chou, F. C. Sodium-ion diffusion and ordering in single-crystal P2-Na_xCoO_2. *Phys. Rev. B: Condens. Matter Mater. Phys.* **2008**, *78*, 052101.

DOI: 10.1021/acs.chemmater.6b01935
Chem. Mater. 2016, 28, 5087−5094